Astron. Astrophys. 324, 981–987 (1997)

ASTRONOMY AND ASTROPHYSICS

Does radius-to-frequency mapping persist close to the pulsar surface?

A. von Hoensbroech[1] **and K.M. Xilouris**[2]

[1] Max-Planck-Institut für Radioastronomie, Auf dem Hügel 69, D-53121 Bonn, Germany
[2] Cornell University, National Astronomy & Ionospheric Center, Arecibo Observatory, P.O. Box 995, Arecibo, PR 00613, USA

Received 14 October 1996 / Accepted 24 February 1997

Abstract. A major uncertainty in our understanding of pulsar emission physics is the location of the radio emission region in pulsar magnetospheres. The narrowing of the intensity profile width with increasing frequency has traditionally been taken as observational evidence supporting a radius-to-frequency mapping in pulsar magnetospheres. Here, 64 high-quality polarimetric profiles at cm-wavelengths have been analyzed to probe for the first time the emission radius at presumably deeper layers of pulsar magnetospheres. Interpreting polarization measurements in the context of the modified relativistic rotating-vector model (Blaskiewicz et al. 1991), we derive emission altitudes and compare our results with the geometrical predictions of a rotating dipolar configuration. We conclude that for slow pulsars the emission is consistent with heights ranging between 1 and 2% of the light-cylinder radius. Only a slight radius-to-frequency mapping is evident at cm-wavelengths which saturates progressively with frequency. The consistency between the results of the two methods further supports the persistence of an undisturbed dipole field throughout the magnetospheres of slow pulsars.

Key words: pulsars: general – pulsars: PSR B0136+57, PSR B0301+19, PSR B0329+54, PSR B0355+54, PSR B0450+55, PSR B0525+21, PSR B0540+23, PSR B0740–28, PSR B0809+74, PSR B0823+26, PSR B0919+06, PSR B0950+08, PSR B1133+16, PSR B1237+35, PSR B1642–03, PSR B1822–09, PSR B1915+13, PSR B1929+10, PSR B1946+35, PSR B2016+28, PSR B2020+28, PSR B2154+40, PSR B2021+51, PSR B2045–16, PSR B2310+42, PSR B2319+60, PSR B2351+61 – polarization

1. Introduction

The narrowing of pulsar integrated profiles with increasing radio frequency suggests that the radiation is emitted from slightly different altitudes over the magnetic poles. In the model proposed by Ruderman & Sutherland (1975), the radiation is related to the local plasma frequency and therefore, to the particle density. In a dipole field, the spreading of open field lines with increasing radius can account for the observed frequency dependence of the profile widths if a radius-to-frequency mapping (RFM) is assumed (Cordes 1978). The detailed form of such mapping depends on the physics of the actual mechanism, although a power-law dependency is typically assumed with an exponent ranging from 0 (no RFM e.g. Barnard & Arons 1986) to –2/3 (Ruderman & Sutherland 1975). Observationally, it is uncertain if a RFM exists, but this simplified model has served reasonably well in interpreting the bulk of observational pulsar data.

Previous attempts to derive emission heights have used a number of techniques including pulsar timing, scintillations, pulse-width narrowing and polarization. Pulsar timing techniques place the emission at a few percent of the light cylinder (Cordes 1978), while scintillation studies of double component profiles yield similar results (Smirnova 1996). Rankin (1990), has examined the pulse widths of core components of orthogonal rotators. Her analysis showed that the emission originates very close to the stellar surface, with different components of the profile originating from different altitudes. In contrast, Gil (1991) has suggested that the emission region is located at the same height for all components of a profile and that it is slightly further away from the surface. While most studies have been carried out at decimetric and meter wavelengths (e.g. Thorsett 1990), very little is known about centimetric and shorter wavelengths. Previous results (Xilouris et al. 1996) have shown that the narrowing of the profile continues to higher frequencies, but approaches progressively a limit where further development is hardly noticed. This narrowing is directly related to the emission altitude, which suggests that at higher frequencies the radio-emission originates from either the same layer or from layers which are packed closely together. This also indicates that at higher frequencies, the emission is not necessarily narrow-band. The mapping of profile widths to emission heights assumes dipolar field geometry where the viewing geometry of the system has to be specified. However, this often cannot be unambiguously determined as we will demonstrate below.

An independent procedure with significant advantages for estimating emission heights has been developed by Blask-

Send offprint requests to: A. von Hoensbroech (avh@mpifr-bonn.mpg.de)

iewicz et al. (1991, hereafter BCW). They extended the familiar rotating-vector model (RVM) of pulsar polarization (e.g. Manchester & Taylor 1977) to include first-order special-relativistic effects. Their model predicts a time lag between the centroid of the total intensity profile and the pulse phase at which the derivative of the polarization position angle (PPA) curve is at a maximum. The emission height r_{em} and this time lag Δt are related by:

$$r_{em} \simeq \frac{c}{4} \cdot \Delta t. \quad (1)$$

Contrary to the pulsar timing methods used earlier, the BCW method can provide absolute emission altitudes. Using actual polarization data, BCW derived an emission height of r_{em} = 300 ± 200 km for 18 pulsars at 1418 MHz, and r_{em} = 410 ± 260 km for 14 pulsars at 430 MHz.

In this work, we used high-quality polarimetry data at the highest frequencies available to trace the RFM towards the deepest layers of pulsar magnetospheres. For these regions evidence has been presented (e.g. Xilouris et al. 1996) that the character of some emission properties undergoes a change. Consequently, probing such regions contributes to our understanding of the emission processes involved closer to the stellar surface. As shown in the following sections, it is necessary to use high-quality data in order to determine accurately the centroid of the profile and the steepest point of the PPA curve. Here, we shall concentrate on the procedures followed to estimate emission heights according to the BCW method and shall compare our results with those derived by assuming a simple dipole configuration. The analysis that ensures the high quality of the polarimetry involved is presented in an accompanying paper (von Hoensbroech & Xilouris 1997), together with the measured polarization profiles.

2. The observations and data analysis

The strongest non-millisecond pulsars observable by the Effelsberg 100-m radio telescope have been monitored in full polarization between November 1993 and November 1995. Three different receivers with center frequencies between 1.4 and 10.5 GHz have been used. With a system temperature of $T_{sys} \simeq 28K$, the prime-focus receiver was tunable from 1.3 to 1.7 GHz, providing a 40-MHz bandwidth and dual polarization. An on-line dedisperser was used to counteract the distortion introduced to the pulsar signal by the interstellar medium. When dedispersion was not needed, a bandwidth between 80 and 200 MHz could be selected. For all the receivers, right-hand (RHC) and left-hand (LHC) circularly polarized components are separated by the polarizer. The signals are then either detected in a multiplying polarimeter or, when performing on-line dedispersion, processed in an adding polarimeter and then detected in a dedisperser (see Seiradakis et al. 1995 for a full description of the observing system). The 4.9-GHz system, recently installed at Effelsberg, provides a bandwidth of 500 MHz and a system temperature of $T_{sys} \simeq 30K$. The polarization is detected in broad-band multiplying polarimeters. The 10.5-GHz receiver has a 300-MHz bandwidth and a system temperature of $T_{sys} \simeq 50K$. All four Stokes parameters are sampled with milliperiod resolution. The signals are calibrated using a polarized noise-diode injected before the polarizer and switched synchronously with the pulsar period. The precise calibration method for both the multiplying and the adding polarimeter, is described by von Hoensbroech & Xilouris (1997). The polarization data presented here has been corrected for cross-coupling errors using the method developed by Xilouris (1991).

2.1. Determining the profile centroid

The BCW method requires the pulse phase of the profile centroid to be determined and compared with the pulse phase of the steepest point of the PPA curve. The phase difference between these two positions directly reflects the emission height at the frequency of observation through Eq. (1).

To determine the profile centroid, several methods have been proposed. In the method we have employed, the boundaries of the pulse profile were determined with the following procedure: First the lowest level of significant emission ($\geq 3\sigma$) is identified on the weakest of the outer components composing the profile. The intensity level at this boundary phase is calculated relative to the component peak. Then the boundary of the opposite outer component is marked at the position where the same relative intensity level is located. An example involving a double component profile is shown in Fig. 1. Although the real boundaries of the profile (the physical edges of the emission region) are not necessarily found with this method, the selection of the points representing the profile boundaries is such that they should have the same distance to the true boundaries. This assumes a homogeneous distribution of the radiation above the polar cap. Following an averaging of the positions of the component boundaries, the real centroid is found. The error of the boundary positions was estimated by:

$$\Delta\phi_{outerpoints} \simeq \frac{rms}{\frac{\delta I}{\delta \phi}}, \quad (2)$$

where rms represents the noise level, and the denominator is the gradient of the profile at the position of each boundary phase.

2.2. Determining the steepest point of the PPA curve

The swing of the PPA curve is theoretically described by the *Radhakrishnan-Cooke curve*, as formulated by the Rotating Vector Model (RVM) (e.g. Manchester & Taylor 1977):

$$\psi = \psi_0 + \arctan\left(\frac{\sin\alpha \sin(\phi - \phi_0)}{\sin\sigma + [1 - \cos(\phi - \phi_0)]\cos\beta \sin\alpha}\right). \quad (3)$$

Here ψ is the polarization position angle, ψ_0 an offset, α the angle between the rotation axis and the magnetic axis (*magnetic inclination*), β the angle between the rotation axis and the line of sight, $\sigma = \beta - \alpha$ is the *impact parameter* representing the angle between the magnetic axis and the line of sight, and ϕ the rotation phase with an offset ϕ_0.

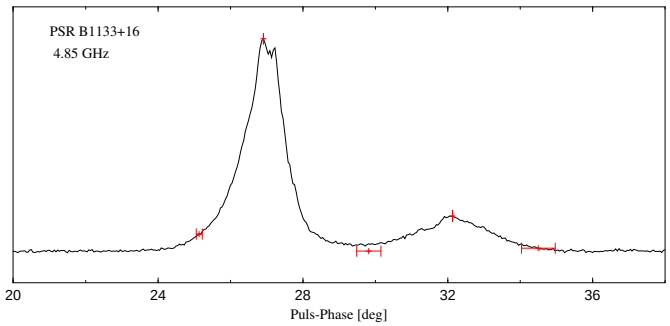

Fig. 1. Determination of the profile centroid for PSR B1133+16. The intensity at the 3σ-level above the baseline, marks the profile boundaries, which for this pulsar correspond to 8% of the intensity of the trailing component peak. The profile centroid, calculated as the average of the profile boundaries, as well as the component peaks are also marked.

This function was fitted to the measured PPA curve using two different numerical algorithms. First, the robust Simplex Algorithm (Nelder & Mead 1965) was applied to get close to the minimum of χ^2. The minimum was then optimized with the Levenberg-Marquart Algorithm (Marquart 1963), which is a more accurate approach, but is very sensitive to the initial parameters.

The goodness of each fit was tested using certain statistical methods: (i) the classical χ^2-test was made, (ii) the post-fit residuals were compared with a Gaussian distribution of equal width using a Kolmogorov-Smirnov test (e.g. Press et al. 1992), and (iii) a post-fit histogram was constructed to verify that the residuals are distributed symmetrically around the fit. This third test is the most stringent since the previous two assume only pure Gaussian statistics. It became evident during the data analysis that the PPA curve often showed systematic deviations from the RVM model thus, making the fitting procedure difficult and the results erroneous.

The pulse phase at which the steepest slope of the PPA curve occurs was derived analytically by zeroing the second derivative of Eq. (3) with respect to the pulse phase ϕ. The error of this point was estimated as in Eq. (2).

2.3. Determining the emission height

Following the estimate of the phase at which the pulse centroid occurs ($t_{profile}$) and that at which the second derivative of the position angle goes to zero (t_{PPA}), the emission height was derived using Eq. (1):

$$r_{delay} \simeq \frac{c}{4} \cdot (t_{PPA} - t_{profile}).$$

The errors were estimated by:

$$\Delta r_{delay} = \frac{c}{4} \cdot \sqrt{\Delta t^2_{PPA} + \Delta t^2_{profile}}. \quad (4)$$

A comparison of our results with emission altitudes calculated using measured pulse widths and a geometrical approach involving a dipole field configuration follows. The geometrical method requires a knowledge of the viewing geometry of the system, namely the magnetic inclination angle α, and the impact parameter σ. To obtain these angles, we fit the observed PPA curves with the RVM. The geometrical emission height was then calculated using the formula (Phillips 1992):

$$r_{geo} \simeq \frac{4}{9}\frac{c}{\Omega}\left[\frac{w^2}{4}\sin\alpha\sin(\alpha+\sigma)+\sigma^2\right], \quad (5)$$

with error

$$\Delta r = \frac{2}{9}\frac{c}{\Omega} w \sin\alpha \sin(\alpha+\sigma)\Delta w, \quad (6)$$

where Ω is the angular velocity, and w the pulse width. This calculation assumes that σ is small and that angles are expressed in radians.

2.4. An evaluation of the BCW method

Though the BCW method provided good results that confirm its value in estimating emission heights, there were a number of problems encountered during the reduction procedure that merit discussion. It is well established that depolarization of pulsar emission occurs at high frequencies (e.g Xilouris et al. 1995). The low signal-to-noise ratios imposed by this depolarization at high frequencies leads to a broad scatter in the values of the PPA curve thus, making the fitting procedure difficult. Furthermore, due to the profile narrowing with increasing frequency the PPA curve is defined at progressively less pulse-phases, biasing the fit results at very high frequencies. PSR B0329+54 for instance, which is known to be one of the brightest pulsars, is severely depolarized with frequency and also exhibits a PPA curve which is hard to analyze. Frequent deviations of the PPA curve from the rotating vector model, which are non-statistical in nature, bias the fitting. For example, orthogonal or quasi-orthogonal moding activity, where a sudden discontinuity of 90° or less appears in the PPA curve, disturbs its otherwise monotonic behavior. This activity has been difficult to explain (e.g. Beskin et al. 1988; Stinebring et al. 1984) although it may originate from competition between different intensity radiation modes emanating from the same or from different heights in the magnetosphere. The competition between the modes results in a perturbed PPA curve which can not be easily fit. Thus, pulse phases that indicate moding activity have been excluded from the fit. In other cases such as PSR B1822–09 or PSR B0450+55, the PPA curve separates into two distinct curves, each corresponding to distinct parts of the intensity profile (see von Hoensbroech & Xilouris subm. 1997). Evidently, it is not possible to apply the BCW method, when the PPA curves are that severely disturbed.

While disturbances in the PPA curve pose difficulties in using the BCW method, to derive the emission heights, the geometrical approach traditionally used also has its problems. There is often a certain ambiguity in the determination of the angles α and β that describe the viewing geometry of the system. (Fig. 2 shows an example for a χ^2-topography.) Here, the best fit occurs where χ^2 reaches a minimum. Evidently, there are a number of

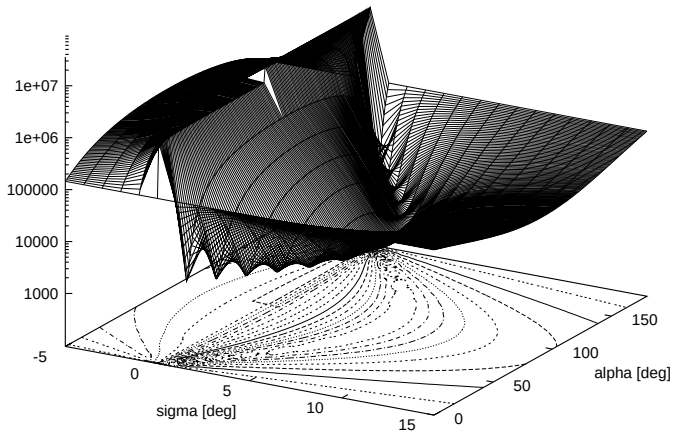

Fig. 2. An example of the χ^2-topography (PSR B1133+16 at 1.4 GHz). Here the value of χ^2 is plotted against α and σ. Evidently, α and σ are highly correlated resulting in an ambiguity in the determination of α.

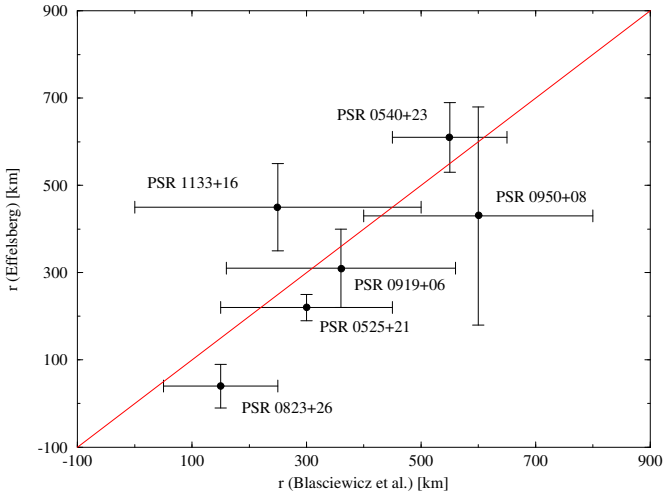

Fig. 3. Comparison of Effelsberg emission altitudes at 1.4 GHz with those from BCW at the same frequency. Those measurements yielding points which lie within 1 σ from the diagonal are naturally consistent.

combinations of α and β which give equally acceptable fits. This shows that the angles derived do not necessarily represent the actual geometry of the system. Such an uncertainty makes the emission heights derived by geometrical methods somewhat doubtful. This ambiguity does not occur for the BCW method as it depends only on the position of the steepest gradient of the PPA curve which can be found without knowing the *real* values of α and β.

3. Results and discussion

A sample of 64 polarimetry profiles at four frequencies was processed. Reasonable fits to the PPA curve were derived in 41 cases. The phase of the steepest gradient of the PPA curve was found to lag the phase of the profile centroid by more than 1 σ in 31 cases. This is in good agreement with the theoretical predictions of the BCW model. In 7 cases, the lags are consistent with zero, and only for two profiles of PSR B2319+60, the PPA is found to lead the profile. Therefore, we find with a certainty of 99% that the PPA swing lags the profile. There are six pulsars in common with the sample of BCW at 1.4 GHz. A comparison is shown in Fig. 3. Within the measurement errors the determination of the emission height is consistent in all six cases. Therefore, in our sample we have included the 430-MHz emission altitudes as derived by BCW for these common sources.

Most of the emission heights that we have derived using the BCW method appear to lie within the first hundred stellar radii or within $1-2\%$ of the light cylinder radius. This is in good agreement with the recent results of timing techniques at high frequencies (Kramer et al. 1997). Our results support the idea that the radio emission originates rather close to the stellar surface. The individual emission altitudes are presented in Table 1 where the derived viewing angles α and σ are also listed. The errors for these angles were estimated from the χ^2-topography. As α and σ are highly correlated, the errors often appear relatively large. he altitudes derived with the geometrical method are also presented for comparison. We have found that in most cases the altitudes estimated with both methods are consistent within two standard deviations or so. This consistency gives further support to the applicability of the BCW method. Due to the ambiguity in the determination of the magnetic inclination angle and the impact parameter (see 2.4), we have also estimated the emission altitudes assuming an orthogonal rotator geometry (α=90°). If such a geometry is assumed, a better correlation between the altitudes estimated by the two different methods is found. The orthogonal rotator geometry, usually leads to an overestimation of the emission height. On the same time, due to the limited accuracy of the pulse-width measurement, the geometrical method tends to underestimate the emission altitude. These two assumptions in the geometrical method counteract each other resulting in a better correlation between the geometrically calculated emission altitudes and that of the BCW method.

The 21 pulsars in our sample have been divided into two groups following the core-conal classification scheme developed by Rankin (1993a and b). Under this scheme, profiles possessing core components are identified with emission primarily from regions closer to the magnetic axis, while conal components represent emission closer to the last open field lines of a rotating dipole configuration. For each group, a histogram was plotted for the distribution of emission heights (Fig. 4). The average emission altitudes are $\bar{r}_{core}$ = 210 $\pm$ 180 km and $\bar{r}_{cone}$ = 420 $\pm$ 200 km respectively. These values are consistent within the errors, providing very weak evidence that the core-emission may originate somewhat closer to the pulsar surface. A Kolmogorov-Smirnov test shows that the two groups possess different distributions with a probability of more than 95%. This supports the idea that there might be a slight difference in the distribution of the emission heights between these classes, as

Table 1. Derived fit parameters and emission altitudes. The values at 0.43 GHz are taken from (Blaskiewicz et al, 1991). r_{delay} are the emission altitudes derived with the BCW method, r_{geo} those from a geometrical method.

Pulsar	Freq. [GHz]	$\alpha[^\circ]$	$\sigma[^\circ]$	r_{delay} [km]	r_{geo} [km]	r_{geo}^{1} [km]
PSR B0136+57	4.85	96.0 ± 15.0	-3.6 ± 15.0	530 ± 74	86 ± 19	87 ± 19
PSR B0301+19	4.85	94.3 ± 15.0	-13.9 ± 15.0	1416 ± 888	2021 ± 246	2130 ± 252
PSR B0329+54	10.45	94.0 ± 15.0	-12.4 ± 15.0	-23 ± 192	1273 ± 86	1279 ± 85
PSR B0355+54	1.71	53.1 ± 80.0	-8.6 ± 4.0	303 ± 76	327 ± 43	429 ± 60
	4.85	155.8 ± 80.0	-2.7 ± 4.0	214 ± 120	50 ± 13	293 ± 88
	10.45	111.9 ± 80.0	-10.2 ± 6.0	128 ± 211	296 ± 113	345 ± 141
PSR B0525+21	0.43	40.0 ± 9.0	1.0 ± 0.2	230 ± 80	1200 ± 300	
	1.41	135.8 ± 60.0	1.3 ± 0.2	224 ± 31	1072 ± 4	2218 ± 10
	1.71	66.3 ± 80.0	2.0 ± 1.0	736 ± 467	1883 ± 144	2194 ± 169
	4.85	17.8 ± 70.0	0.6 ± 2.0	378 ± 174	175 ± 5	1731 ± 53
PSR B0535+28	1.41	108.5 ± 30.0	-11.5 ± 6.0	619 ± 96	315 ± 58	323 ± 61
	4.85	79.5 ± 15.0	-18.5 ± 15.0	240 ± 267	516 ± 142	537 ± 157
PSR B0540+23	0.43	125.0 ± 12.0	-14.0 ± 1.0	850 ± 100	230 ± 200	
	1.41	162.5 ± 80.0	-3.5 ± 6.0	612 ± 81	45 ± 3	381 ± 52
	4.85	80.3 ± 20.0	10.0 ± 10.0	730 ± 155	489 ± 94	488 ± 94
	10.45	101.1 ± 90.0	-8.3 ± 6.0	297 ± 167	277 ± 61	279 ± 61
PSR B0740-28	1.41	96.2 ± 20.0	-16.0 ± 15.0	210 ± 29	371 ± 12	369 ± 11
	4.85	78.2 ± 15.0	14.8 ± 15.0	268 ± 38	349 ± 16	347 ± 16
	10.45	47.3 ± 90.0	-6.9 ± 5.0	225 ± 218	77 ± 32	105 ± 66
PSR B0809+74	1.71	93.4 ± 10.0	-9.8 ± 15.0	1267 ± 438	2420 ± 259	2409 ± 258
	4.85	174.3 ± 90.0	$-.7 \pm 7.5$	447 ± 725	21 ± 3	1498 ± 309
PSR B0823+26	0.43	79.0 ± 1.0	3.2 ± 0.3	150 ± 100	100 ± 10	
	1.41	89.8 ± 25.0	1.0 ± 0.2	37 ± 53	78 ± 10	78 ± 10
	1.71	82.3 ± 80.0	1.7 ± 1.5	107 ± 67	65 ± 11	65 ± 11
	4.85	97.5 ± 15.0	-12.1 ± 15.0	80 ± 21	583 ± 4	582 ± 4
PSR B0919+06	0.43	45.0 ± 200.0	5.0 ± 16.0	760 ± 140	390 ± 100	
	1.71	90.4 ± 80.0	2.9 ± 2.0	314 ± 87	100 ± 20	100 ± 20
	4.85	48.0 ± 80.0	2.9 ± 2.5	247 ± 68	50 ± 6	69 ± 12
PSR B0950+08	0.43	6.0 ± 90.0	-2.5 ± 40.0	600 ± 200	20 ± 600	
	1.41	$-.7 \pm 5.0$	1.0 ± 15.0	432 ± 249	1 ± 1	1545 ± 220
	4.85	-26.9 ± 90.0	4.1 ± 5.0	159 ± 348	164 ± 56	802 ± 323
PSR B1133+16	0.43	147.0 ± 110.0	3.0 ± 10.0	250 ± 250	600 ± 600	
	1.41	26.9 ± 90.0	2.8 ± 4.4	452 ± 102	122 ± 1	335 ± 4
	1.71	103.6 ± 80.0	4.1 ± 2.5	505 ± 146	330 ± 7	345 ± 7
	4.85	33.0 ± 80.0	3.1 ± 4.0	426 ± 165	122 ± 4	233 ± 14
PSR B1915+13	4.85	90.7 ± 12.5	-9.3 ± 15.0	346 ± 75	236 ± 32	236 ± 32
PSR B1946+35	4.85	52.9 ± 80.0	4.2 ± 3.0	133 ± 168	353 ± 41	485 ± 61
PSR B2016+28	4.85	89.8 ± 15.0	4.2 ± 15.0	159 ± 181	270 ± 48	270 ± 48
PSR B2021+51	1.41	22.5 ± 90.0	1.2 ± 2.5	787 ± 42	60 ± 2	370 ± 19
	1.71	21.0 ± 80.0	3.1 ± 5.0	450 ± 91	82 ± 5	369 ± 38
	4.85	22.4 ± 90.0	4.0 ± 5.0	389 ± 137	108 ± 9	373 ± 55
	10.45	87.9 ± 80.0	5.8 ± 3.0	590 ± 182	251 ± 50	251 ± 49
PSR B2045-16	4.85	89.5 ± 15.0	-1.5 ± 15.0	443 ± 232	666 ± 36	667 ± 36
PSR B2154+40	4.85	101.1 ± 15.0	-16.0 ± 15.0	904 ± 470	3983 ± 239	3959 ± 235
PSR B2319+40	1.41	102.3 ± 80.0	-8.1 ± 4.0	-418 ± 223	2845 ± 93	2875 ± 94
	4.85	89.9 ± 15.0	-6.5 ± 15.0	-1242 ± 540	2201 ± 239	2201 ± 239
PSR B2351+61	1.41	61.2 ± 80.0	-2.9 ± 2.0	379 ± 241	204 ± 45	257 ± 60

[1] upper limit with $\alpha = 90^\circ$.

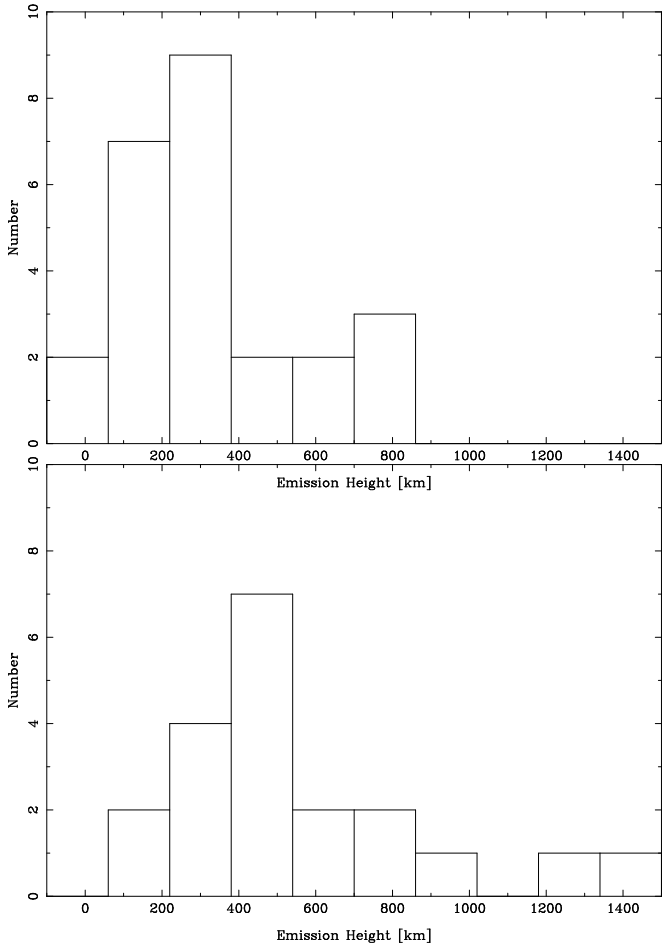

Fig. 4. Emission radii histograms for core (*upper panel*), and conal component dominated profiles (*lower panel*)

initially suggested by Rankin (1990). However, more data is necessary for a statistically supported argument.

3.1. Radius-to-frequency mapping

A power-law fit to the emission altitudes derived with the BCW method as a function of frequency was done for each pulsar. A radius-to-frequency mapping (RFM) assuming the power law, $r \propto \nu^a$, was derived for each pulsar. The results for the individual pulsars are listed in Table 2. The significant scatter in the values of the exponent suggests that each pulsar is described by its own RFM. Typically, the exponent is negative which implies that higher frequencies originate from lower emission altitudes. Exceptions are PSR B0525+21 and PSR B0740–28, where the exponents are positive. The case of PSR B0525+21, is consistent with Phillips (1991) who derived a positive exponent using the timing method. However, in both cases, the exponent is also consistent with zero within slightly more than one σ. An average value of the RFM exponent was calculated at these frequencies by averaging the emission altitudes at each frequency and fitting a power law to the mean values. This leads to an average value for the exponent of $\bar{a} = -0.3 \pm 0.1$.

Table 2. Radius-to-frequency mapping exponent a with 1σ errors.

Pulsar	a
PSR B0355+54	-0.39 ± 0.38
PSR B0525+21	$+0.21 \pm 0.19$
PSR B0535+28	-0.77 ± 0.62
PSR B0540+23	-0.15 ± 0.08
PSR B0740–28	$+0.18 \pm 0.15$
PSR B0809+74	-0.99 ± 0.97
PSR B0823+26	-0.21 ± 0.22
PSR B0919+06	-0.49 ± 0.12
PSR B0950+08	-0.40 ± 0.35
PSR B1133+16	$+0.07 \pm 0.26$
PSR B2021+51	-0.26 ± 0.12

4. Conclusions

A time delay between the centroid of the intensity profile and the steepest point of the PPA swing has been predicted by Blaskiewicz et al. (1991). This delay is directly proportional to the emission altitude. In comparison with other methods previously used, this approach has significant advantages since it entails fewer assumptions. In particular, the viewing geometry of the system is not required. Further, the determination of the profile centroid does not require knowledge of the physical boundaries of the relevant radiation zones. While this method seems less model dependent, it is severely restricted by the deviations often encountered in the PPA curve in the form of either orthogonal or quasi-orthogonal moding activity.

A sample of 64 profiles has been processed using the BCW method, and in 41 cases, reasonable fits were possible. Among those well-established fits, the PPA curve indeed lags the profile centroid, for more than 90% of the cases. This gives further support to the BCW method. Further, our results are found to be consistent with those of BCW which demonstrates the repeatability of the method. The derived emission altitudes have been compared with those calculated by geometrical methods. Within the errors most of the altitudes were found to be consistent. This consistency supports the persistence of an undisturbed dipolar magnetic field configuration throughout the magnetospheres of slow pulsars.

The emission appears to originate from regions very close to the pulsar surface (1-2% of the light-cylinder radius). The pulsars have been divided into those with core-dominated and those with mainly conal-dominated profiles using the classification of Rankin (1993a and b). Weak evidence is presented that the core-dominated profiles may originate slightly closer to the surface: Average values are r_{core} = 210 $\pm$ 180 km for core-dominated, and r_{cone} = 420 $\pm$ 200 km for cone-dominated profiles. Using a Kolmogorov-Smirnov test, it has been shown that the probability of the two distributions being drawn from the same parent distribution is less than 5%.

Further investigation of the RFM was made by assuming a power-law dependence $r \propto \nu^a$. While individual sources behave in very different ways, most show a tendency for decreasing emission altitudes with higher frequencies. Notable exceptions are PSR B0525+21 and PSR B0740–28, where the emission altitude has been found to increase with frequency.

The large scatter among the derived RFM exponents could be due to a saturation towards higher frequencies. However, the average RFM may be more significant. The average emission altitudes at each frequency are fit by a power law with $\bar{a} = -0.3 \pm 0.1$ which suggests a weak radius-to-frequency mapping.

Acknowledgements. We wish to thank R. Wielebinski, A. Jessner, M. Kramer, H. Lesch and C. Salter for their constant interest in this work and all their helpful comments. Arecibo Observatory is operated by Cornell University under cooperative agreement with the National Science Foundation.

References

Barnard J.J., Arons J., 1986, ApJ, 302, 138
Beskin V.S., Gurevich A.V., Istomin Y.N., 1988, SvA, L14, 93
Blaskiewicz M., Cordes J.M., Wasserman I., 1991, ApJ, 370, 643 (BCW)
Cordes J.M., 1978, ApJ, 222, 1006
Gil J.A., 1991, A&A, 243, 219
von Hoensbroech A., Xilouris K.M., 1997, *accepted*
Kramer M., Xilouris K.M., Jessner A. et al., 1997, *in press*
Manchester R.N., Taylor J.H., 1977, Pulsars, Freeman, San Francisco
Marquart D.W., 1963, J. Soc. Ind. Apll. Math., 11, 431
Nelder F.C., Mead R., 1965, Computer Journal, 7, 308
Phillips J.A., 1991, PhD Thesis, Cornell University
Phillips J.A., 1992, ApJ, 385, 282
Press W.H., Teukolsky S.A., Vetterling W.T., Flannery B.P., 1992, Numerical Recipes, Cambridge University Press
Rankin J.M., 1990, ApJ, 352, 247
Rankin J.M., 1993a, ApJ, 405, 285
Rankin J.M., 1993b, ApJS, 85, 145
Ruderman M.A., Sutherland P.G., 1975, ApJ, 196, 51
Seiradakis J.H., Gil J.A., Graham D.A., et al., 1995, A&ASS, 111, 205
Smirnova T.V., Shishov V.I., 1989, SvA, L15, 191
Stinebring D.R., Cordes J.M., Weisberg J.M., et al., 1984, ApJS, 55, 27
Thorsett S.E., 1990, ApJ, 377, 263
Xilouris K.M., 1991, A&A, 248, 323
Xilouris K.M., Kramer M., Jessner A. Wielebinski R., 1996, A&A, 309, 481
Xilouris K.M., Seiradakis J.H., Gil J.A., et al., 1995, A&A, 293, 153

This article was processed by the author using Springer-Verlag LaTeX A&A style file *L-AA* version 3.